Instrument Science Report WFC3 2015-003

WFC3/UVIS Charge Transfer Efficiency 2009 - 2015

S. Baggett, C. Gosmeyer, K. Noeske
March 31, 2015

ABSTRACT

The longterm behavior of the charge transfer efficiency (CTE) in WFC3/UVIS is monitored using observations of external star clusters. Flux loss due to CTE degradation is a function of the source's distance from the amplifier, the source signal level, the background within the image, and the epoch of the observations. The worst-case flux losses occur in images with extremely low backgrounds. In such data, based on photometry within a 3-pixel radius aperture and losses measured across 2048 pixels, the flux losses in early 2015 for faint sources (500-2000 e-) can be as high as ~50+/-2%; losses for brighter sources (8000-32000 e-) are considerably less: ~5 +/-1%. Ensuring a modest amount of background can reduce the losses substantially: ~12e-/pix, added via post-flash, reduced the losses to ~15+/-1% and ~4+/-1% for faint and bright sources, respectively. Applying the empirical pixel-based CTE correction algorithm can also reduce flux losses: to ~10+/-1% and ~0+/-1% (unflashed images, no background) and to 3+/-1% and 0.5+/-1% (post-flashed), for the faint and bright sources, respectively. We find that the CTE correction appears to slightly over-correct (1-5%) bright sources in low image backgrounds and over-correct most sources in post-flashed images. We empirically fit the flux losses as a function of source flux, observation date, background level, and distance from the amplifier with a 2nd order polynomial and provide tabulated coefficients.

Introduction

CCD's in low-earth orbit suffer from radiation damage effects due primarily to periodic

passes through the South Atlantic Anomaly (SAA), a region where the Van Allen belts are closest to the Earth, causing an increase in radiation rates. The damage manifests itself in WFC3/UVIS images as a growing population of hot pixels and increasing dark current (e.g. Sect.5.4.8 and 5.4.9 in Dressel et al. 2015) as well as decreasing charge transfer efficiency (CTE), the topic of this report.

CTE is a measure of how well charge is transferred during readout; a perfect device would completely transfer all charge from row to row without losing any during the process. The on-orbit radiation environment, however, generates defects within the silicon matrix of the detector which trap charge during the image readout, resulting in a less-than perfect CTE. The subsequent release of the charge from the traps during readout causes charge 'trails' which point in the direction opposite to the readout, i.e. away from the amplifier. This results in CTE losses, as the total detected flux of the source in an aperture is reduced. Figure 1 presents two image subsections, one as close as possible to the amp and one furthest from the amp, where sources suffer the maximum number of charge transfers, hence the highest CTE loss and thus exhibit significant charge trails. The charge trailing can lead to systematic errors in astrometry, an aspect to be evaluated in a separate study; this report focuses on the effects of CTE losses on the measured flux.

Figure 1. At left, a 1000x1000 pixel image subsection closest to the amplifier which in this case is at lower left. At right, a 1000x1000 pixel image subsection furthest from the amplifier. Neither exposure has had a post-flash applied; the sky background was ~0 e-/pix. The readout direction is marked with an arrow.

In general, the decline in CTE reduces the detected source flux as defects within the pixels trap and release charge during the readout. Those flux losses depend on a variety of factors (Baggett et al., 2011; MacKenty & Smith, 2012; Noeske et al., 2012):

1) *Distance from the amplifier*. Sources far from the amp must traverse more pixels during readout than a source close to the amp, thus encountering more traps and consequently suffering more charge loss.
2) *Signal level*. Fainter sources in WFC3/UVIS images suffer a higher fractional loss than brighter sources (Anderson et al., 2012). Some faint sources may even be smeared completely out of existence. Ensuring a minimum background of 12 e-/pix[1], using post-flash if necessary, can help prevent some of these faint source losses.
3) *Image background*. A higher overall background within the image reduces CTE losses by filling traps before the readout begins. The WFC3 has a low natural background for many modes, with an average dark current of only ~7 e-/hr in 2015, readnoise of ~3 e-, and UV / narrow-band imaging with very low natural sky levels[2]. In the absence of sufficient natural background, observers should use post-flash, as recommended in item 2 above. Details of the efficacy of post-flash for mitigating CTE losses are available in Anderson et al. (2012).
4) *Observing scene*. Sources which precede the target source during the readout fill charge traps and thus could improve the CTE for the target charge packets.
5) *Epoch (time since installation on-orbit)*. The effects of radiation damage to the detector accumulate over time, resulting in ever-increasing loss of CTE.

As an aside, we note that observers can mitigate some of the effects of CTE losses by 1) placing small targets near an amplifier, 2) ensuring a minimum image background (12 e-/pix average as of 2015) via long exposure times and/or application of a post-flash and 3) applying the pixel-based CTE correction. Using the recommended minimum background, observers can keep CTE losses below ~20%, a regime where pixel-based CTE corrections are generally accurate.

In the following sections, we summarize the external CTE monitor data, the method used to analyze the data, and the results, including a section on the performance of the pixel-based CTE correction algorithm.

[1] The recommended background value provides a balance between improving the CTE and minimizing the additional photon noise from the background; improvements to the CTE are minimal with higher backgrounds (Anderson et al. (2012).
[2] Estimated sky backgrounds may be computed using the WFC3 ETC or using the tables in Baggett & Anderson (2012).

Data

The images used in the analysis presented here have been drawn from every WFC3/UVIS external CTE monitor program executed since launch. The proposals and targets are summarized in Table 1. A few notes about the programs follow.

During Cycle 17, only the rich open cluster NGC 6791 was observed. The relative sparseness of the cluster limits the number of stars which fall within a given column which could pre-fill traps and thus reduce CTE losses for sources which follow during the readout. Later cycles include pointings in the globular cluster NGC 104 to provide a more dense field of sources.

Proposal 12348 was not intended as a monitor but a test of the charge injection (CI) mode as a CTE mitigation option (Baggett et al., 2011, Bushouse et al., 2011). However, since the proposal included some baseline non-CI images of one of the standard clusters used for CTE monitoring, we include those images in the analysis here.

Images from visit 13 of proposal 12379 have been removed from the analysis. This particular visit had a guide star acquisition issue which prevented some exposures from being taken and resulted in elliptical PSFs in other exposures.

Post-flash has been found to be more beneficial in mitigating CTE on-board than CI; as a result, the post-flash mode was made available for use in Cycle 20 and the CI mode has been retired. Up until Cycle 20, CTE monitor exposures were taken in F606W and F502N in order to obtain images with high and low backgrounds, respectively. Starting in Cycle 20, the CTE monitor data are in F502N only but taken both with and without post-flash. The unflashed data provide a continuation of the monitoring of CTE losses in low background images while the flashed data provide an efficient means of acquiring images with a variety of background levels.

Table 1.UVIS external CTE monitor observations.

Program	Cycle	Observation Dates	Filters	Target
11924	17	Oct 2009, Mar 2010, Sep 2010	F502N, F606W	NGC 6791
12348	18	Sep 2010	F502N	NGC 104
12379	18	Nov 2010, Mar 2011, Apr 2011	F502N, F606W	NGC 6791, NGC 104
12692	19	Oct 2011, Mar 2012, Jun/Jul 2012	F502N, F606W	NGC 6791, NGC 104

13083	20	Nov 2012, Mar 2013, Jul/Aug 2013	F502N	NGC 6791, NGC 104
13566	21	Jan 2014, Jul 2014	F502N	NGC 6791, NGC 104
14012	22	Feb 2015	F502N	NGC 6791, NGC 104

Observation strategy

Earlier reports of the external CTE monitoring results describe the observing and analysis procedure in detail (Noeske et al., 2012, Khozurina-Platais et al., 2011). We continue the method outlined in those analyses and provide an overview of the procedure here.

An ideal CTE test would consist of contemporaneous observations of a source such as a star cluster both near and far from the amplifier on the same chip. To achieve this with WFC3 would require imaging the cluster, rolling the spacecraft by 180 degrees and imaging the field again. However, due to thermal and power constraints on HST, opportunities to perform such large rolls within a given visit are rare. Instead, to ensure the required monitoring cadence can be achieved with adequate target availability, the basic observing technique is to place the target in one chip, then shift the pointing by about 2000 pixels in Y to place the field into the second chip. Due to the location of the amplifiers in the corners of the field of view, stars which are close to an amplifier in one chip will fall far from an amplifier in the other chip (see Fig 3). The difference in the stellar magnitudes (i.e. ratio of the fluxes) from one chip to another as a function of difference in Y coordinate provides an estimate of the CTE loss. This strategy has been shown to work well (Noeske et al., 2012 Khozurina-Platais et al., 2011) though with the caveat that the measured CTE losses are a blend of the behavior of both chips.

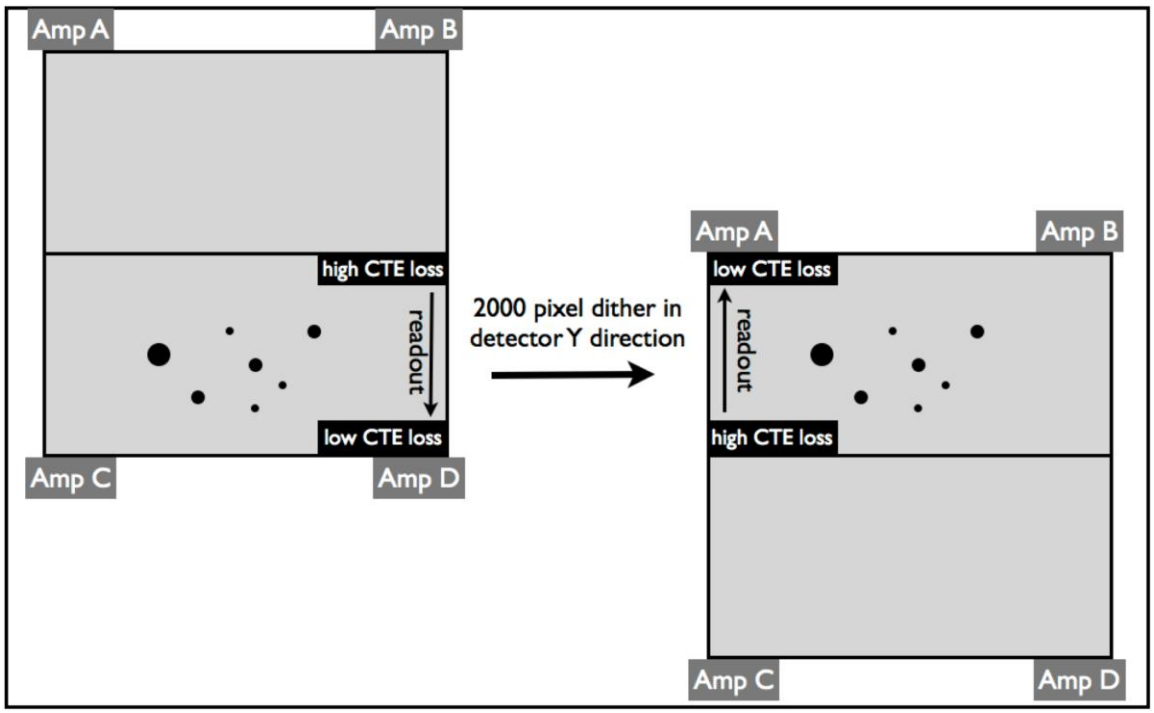

Figure 2. Observing strategy for the external CTE monitors (figure from Noeske et al., 2011)

Image processing

The standard *calwf3* software is used to calibrate the raw images. Corrections include the image overscan, bias, dark, post-flash if applicable, and flatfield. The remainder of the analysis is performed on the resulting *flt.fits files. First, the files are corrected with the pixel area map to account for geometric distortion (~7% in WFC3 from corner to corner). By design, the flatfield correction step in *calwf3* normalizes the image to uniform surface brightness across the field of view and so for accurate point source photometry, flatfielded WFC3 images must be multiplied by the pixel area maps[3].

Daophot in *iraf/pyraf* is used to find sources and perform the aperture photometry. Coordinates for sources are matched across the detectors; stars must match to within a 5-pixel radius and any stars with multiple matches within 4 pixels are discarded. The photometry is measured within a 3-pixel radius aperture; the sky value is taken from a 10-pixel wide annulus with inner radius of 10 pixels. Only stars with photometric errors <0.1 mag are kept in the sample.

Finally, a resistant mean linear fit (*robust_linefit* program in IDL) is performed on the magnitude differences (flux ratios) from chip 1 and chip 2 as a function of row number in chip 2. An example of the magnitude difference plots is shown in Fig 3. Note that the CTE slope in such plots reflects twice the actual CTE loss: stars near or far from amp C in the first image will be far or near an amp in the second image, respectively, and show

[3] The WFC3 pixel area maps are available at http://www.stsci.edu/hst/wfc3/pam/pixel_area_maps.

the maximum CTE loss at the ends of the fit (y~0 and y~2000). Stars in the center of one chip, at y~1000, will be in the center of the second chip after the dither, showing little difference in flux assuming the CTE losses in the two chips are similar.

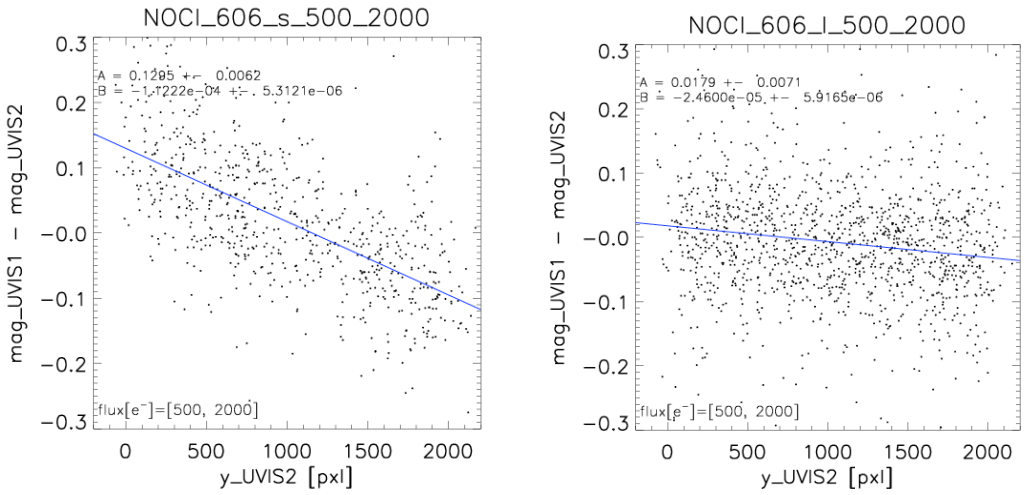

Figure 3. Magnitude differences as a function of chip 2 row number, for faint stars with 500-2000 e- in a 3-pixel radius aperture in images with low background (left) and high background (right). In this case, the CTE losses for sources furthest from the amp amount to ~10% +/-0.5% and ~3%+/-0.5% for low and high background images, respectively.

CTE monitor results

Figure 4 summarizes the measured flux losses due to CTE as a function of time from Oct 2009 through Feb 2015; formal error bars are noted with vertical lines. As discussed earlier, with the advent of the post-flash mode in Cycle 20, the high-background F606W images have been discontinued. Figure 5 summarizes the slopes of the CTE losses as a function of source flux and epoch. The model developed by Noeske et al. (2012) is used to fit the data with a 2nd order polynomial constrained by all flux bins and epochs simultaneously. We find that:

1) Flux losses due to CTE degradation show a smooth evolution over the past 5+ years. There may be some hint of a flattening in the flux losses for intermediate and bright sources over the past ~2 years which would be consistent with radiation levels in the SAA decreasing as solar maximum approaches (Baggett et al., 2011).
2) As expected, flux losses are highest for the fainter sources in Figure 4 (500-2000 e- in 3-pixel radius aperture), approaching ~50% for sources in images with effectively no background.
3) The brightest sources (>10k e- in 3-pixel radius aperture) show the smallest amount of flux losses, up to ~5% in images with low backgrounds and 1-2% in

images with high backgrounds.

4) Even a minimal level of background can provide some mitigation of flux losses in the fainter sources. For example, at MJD~56900 (Sep 2014), a 2-3 e-/pix of background reduces flux losses from ~45% to ~37% (500-2000 e- bin) and from ~22% to ~13% (2000-8000 e- bin). Flux losses from the brightest sources (8000-32000 e-) remain relatively unchanged with the small increase in background.
5) A high image background helps reduce CTE losses considerably. For example, around MJD 56200 (Sep 2012), CTE losses for the faintest sources were ~40% in images with no background and only ~8% in images with 20-30 e-/pix background. Similarly, intermediate flux sources saw reductions in flux losses from 15% with low background to ~5% in images with high background. The most recent data show a maximum of ~15% flux loss for faint sources in images with low backgrounds. We note here that the recommended optimum background for mitigating CTE is currently 12 e-/pix (Anderson et al., 2012); beyond this level, the improvement in CTE flattens and the additional photon noise penalty due to the higher background is no longer warranted.
6) There is no discernable systematic trend for smaller CTE losses in the dense cluster NGC 104 than in the sparse cluster NGC 6791, as might be expected if sources preceding the target source "prefill" the charge traps before the target is readout. This may be due to NGC 104 not being dense enough to ameliorate the CTE losses and/or additional sources of error, such as residual cosmic-ray effects contributing to the CTE slope scatter, are masking the effect.
7) Overall the data are well-fit by the 2nd order polynomial model although there are occasional outliers such as two of the lower flux bins in July 2014 and one of the the higher flux bins in Sep 2010 and July 2012.

We note that in the first 1-2 years of the WFC3 mission, flux losses due to CTE for moderately bright targets (500-2000 e- total flux in 3-pixel radius aperture) were found to be a factor of 2-3 greater than what would have been expected based on the performance of ACS (Advanced Camera for Surveys) during its early lifetime on-orbit (Chiaberge et al., 2009). The difference has been attributed to the solar cycle: the strength of the SAA – and its damaging radiation field – is known to be anti-correlated with solar activity and WFC3 was installed in mid-2009 near solar minimum while ACS was installed in 2002, close to solar maximum (Baggett et al., 2011 and references therein). Consistent with this hypothesis is that ACS experienced more rapid CTE degradation during 2009/2010 (Massey, 2010), the first two years of WFC3 on orbit.

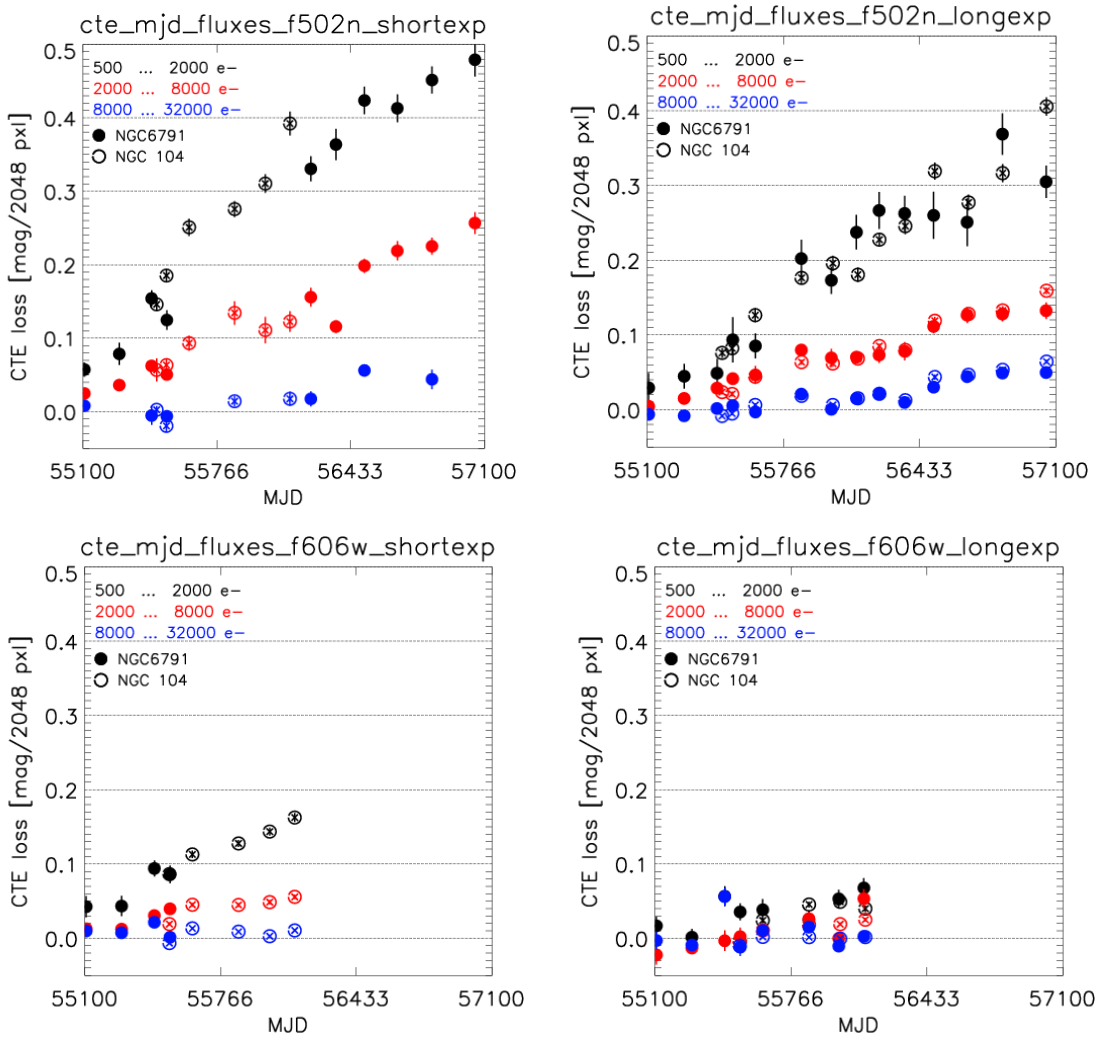

Figure 4. Flux losses per 2048 rows due to CTE degradation as a function of time, from Oct 2009 through Feb 2015 (top) and from Oct 2009 through July 2012 (bottom). Source levels are 500-2000 e- (black), 2000-8000 e- (red), and 8000-32000 e- (blue) within a 3-pixel radius aperture, drawn from the relatively sparse cluster NGC 6791 (filled symbols) and the dense cluster NGC 104 (open circles). Background levels are ~0 e-/pix (upper left), ~1-2 e-/pix (upper right), 2-3 e-/pix (lower left), and 20-30 e-/pix (lower right). The broadband observations (lower plots) have been discontinued since Cycle 20, when the post-flash mode became available.

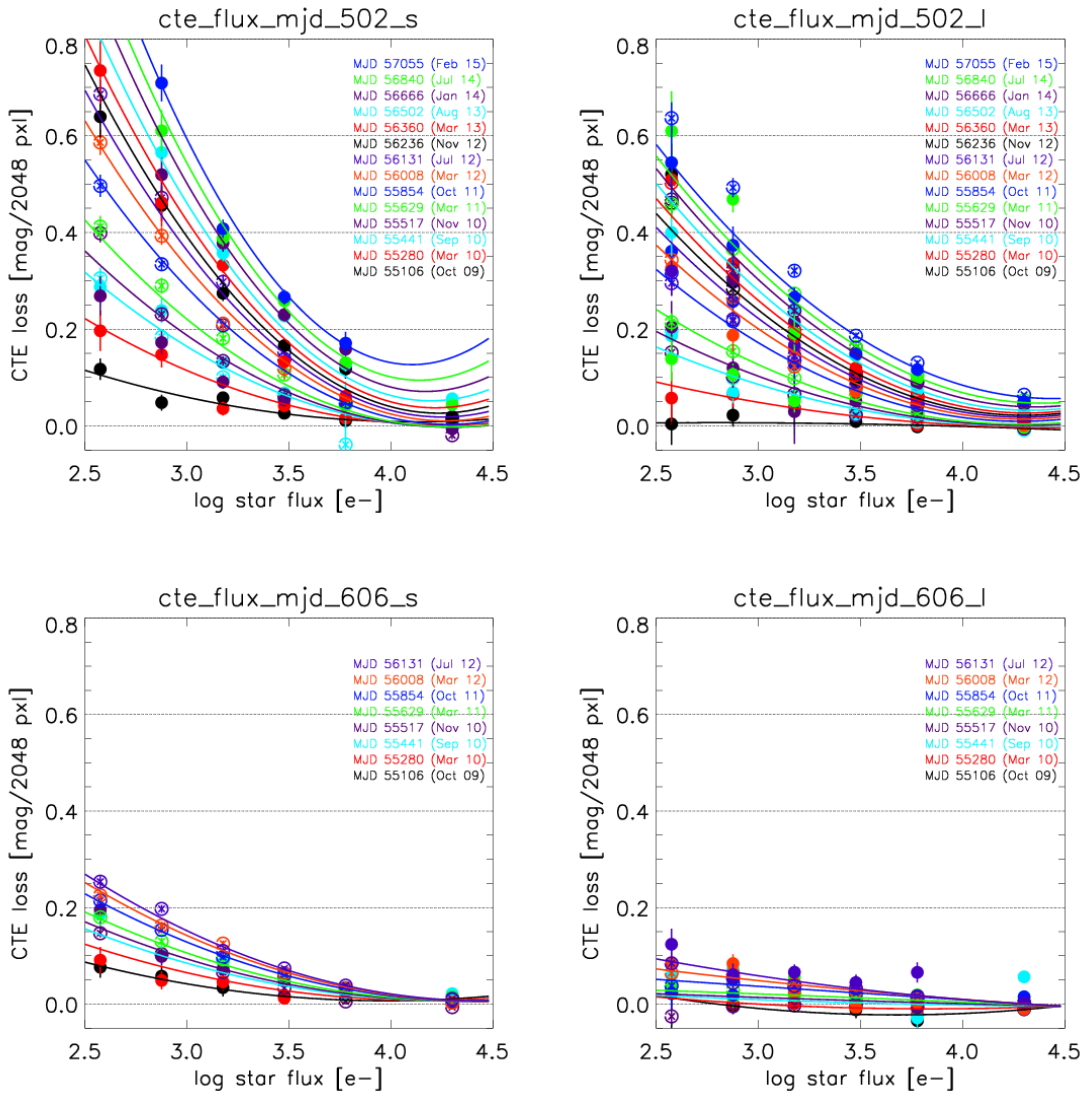

Figure 5. Slope of CTE losses in magnitudes per 2048 rows as a function of source flux, from Oct 2009 through Feb 2015 (top) and July 2012 (bottom) along with the model fits (lines). Each color references a different visit i.e. epoch. As for Figure 4, NGC 6791 and NGC 104 are shown in filled and open symbols, respectively. Background levels are ~0 e-/pix and 1-2 e-/pix (upper left and right), 2-3 e-/pix and 20-30 e-/pix (lower left and right).

Efficacy of post-flash and empirical CTE-correction algorithm

The CTE monitoring data, with its variety of source brightnesses, image backgrounds, and changing levels of CTE losses, provide a convenient test case for the empirical pixel-based CTE correction developed for WFC3. The correction, based on an empirical model of the pixel-by-pixel CTE losses, was developed following the methodology used for ACS (Massey, 2010, Anderson & Bedin, 2010). At the heart of the technique is the use of hot pixels in dark frames with the assumption that hot pixels unaffected by CTE losses are delta functions and thus, any deviation from a delta function represents CTE losses

(Anderson et al., 2012b). The first step in developing the correction was to identify bright warm pixels (i.e., those with relatively large number of counts and small corrections) in long-exposure darks. Those warm pixels were scaled down to estimate their level in short-exposure darks and that level was compared to what the surviving counts were in short darks (where the CTE trails are too faint to measure). The losses were tabulated as a function of warm pixel size and background and a model was fit to the data; that model was inverted to obtain a correction for science images. One caveat with the algorithm is that it can not completely recover what was lost, particularly at the faintest levels. To avoid amplification of read noise, the algorithm is conservative in its reconstruction at the low background levels where losses are highly non-linear.

The CTE correction software is currently available as a standalone FORTRAN routine (available at http://www.stsci.edu/hst/wfc3/tools/cte_tools). It operates on the raw files and produces CTE-corrected raw files and, if given flt files, also produces CTE-corrected calibrated files. The CTE correction is currently being implemented into the standard *calwf3* pipeline and is expected to be installed in the STScI automated data processing pipeline before the end of 2015 (Baggett et al., 2014).

The CTE monitor data have been processed through the correction script to produce CTE-corrected calibrated files (*flc) which were then processed through the standard monitor procedure to obtain CTE loss plots as a function of MJD. Shown in Fig 6 is the case for the narrowband F502N images. The results can be summarized as follows.

1) *Pixel-based CTE-correction, no post-flash (i.e. low background).* The correction code is able to reduce flux losses due to CTE from ~35% to ~10% for the faintest sources in this study, 500-2000 e- within a 3-pixel radius aperture. Intermediate sources see reductions in losses from ~12% to ~2% while the brightest sources see reduction from ~5% down to ~0. There are some epochs for which the CTE correction appears to slightly overcorrect the intermediate and bright sources (by a few %).
2) *Post-flash only, no CTE correction.* The flash reduces flux losses for faint sources from ~35% down to ~15%. Intermediate and bright sources see smaller benefits: flux losses of ~13% and 5% are reduced to ~8% and 4%, respectively.
3) *Post-flash plus pixel-based CTE correction.* The combination of postflash plus the CTE correction results in the most dramatic improvement. The algorithm appears to slightly over-correct most data by a few percent.

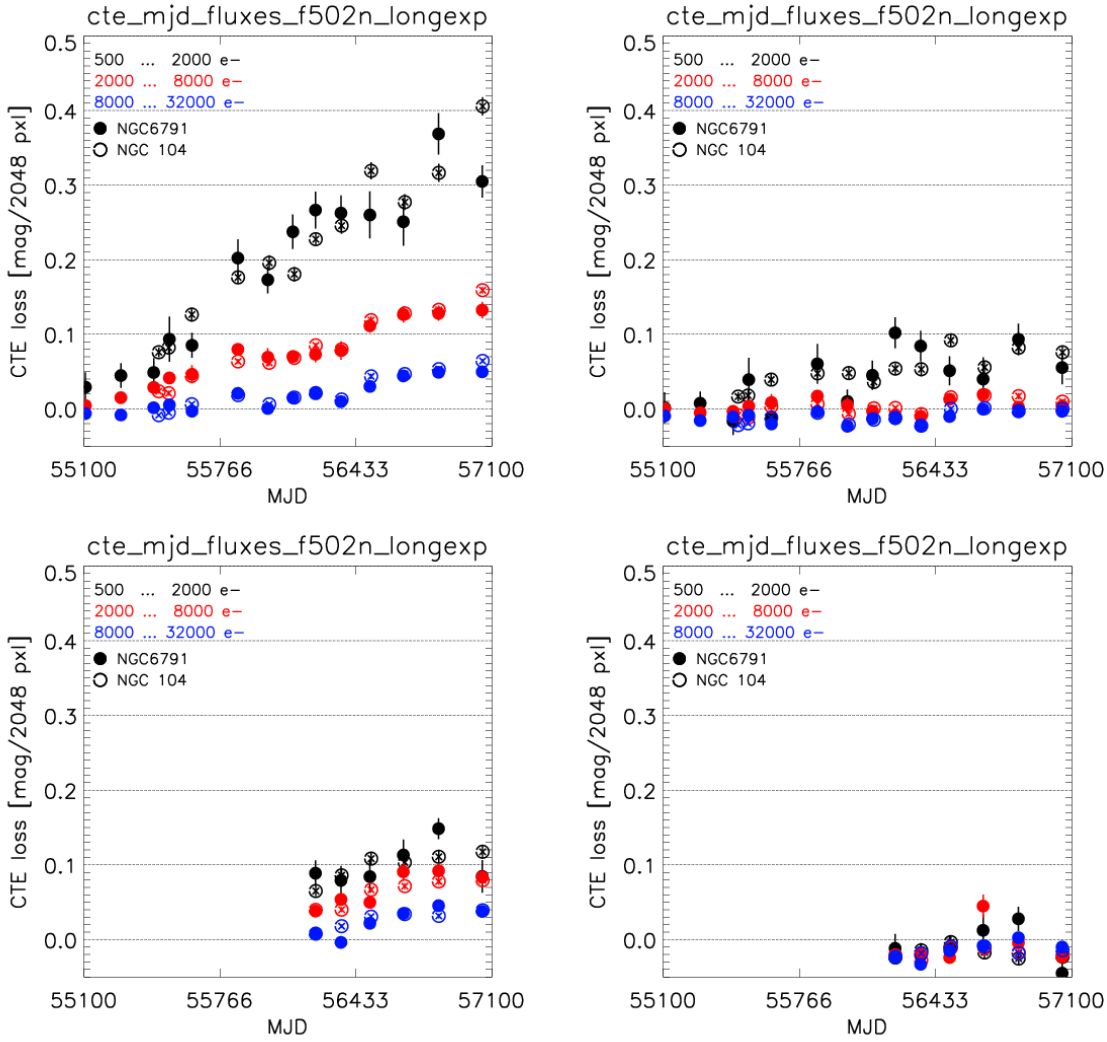

Figure 6. Reduction of CTE losses for narrowband images (very low background). At upper left are the baseline CTE monitor results, i.e. no corrections are applied (same as in Fig 4). At upper right, the monitor data have been processed through the CTE-correction software. At lower left and right respectively, data have been post-flashed and post-flashed plus CTE-corrected. The observations for the bottom row of plots start in Cycle 20 when post-flash became available. Note that for the standard CTE monitoring, un-flashed data continue to be acquired in addition to post-flashed images.

Figure 7 illustrates the efficacy of the pixel-based CTE correction on the broadband F606W images. As for the F502N data, these CTE images have been processed through the correction script to produce CTE-corrected calibrated files (*flc) which were then processed through the standard monitor procedure to obtain CTE loss plots as a function of MJD. For CTE losses originally higher than ~10%, the correction is able to reduce those losses down to ~3%. Similar to the results for the F502N data, we find that once CTE losses are less than ~10%, the CTE correction algorithm appears to over-correct the observed fluxes by a few percent.

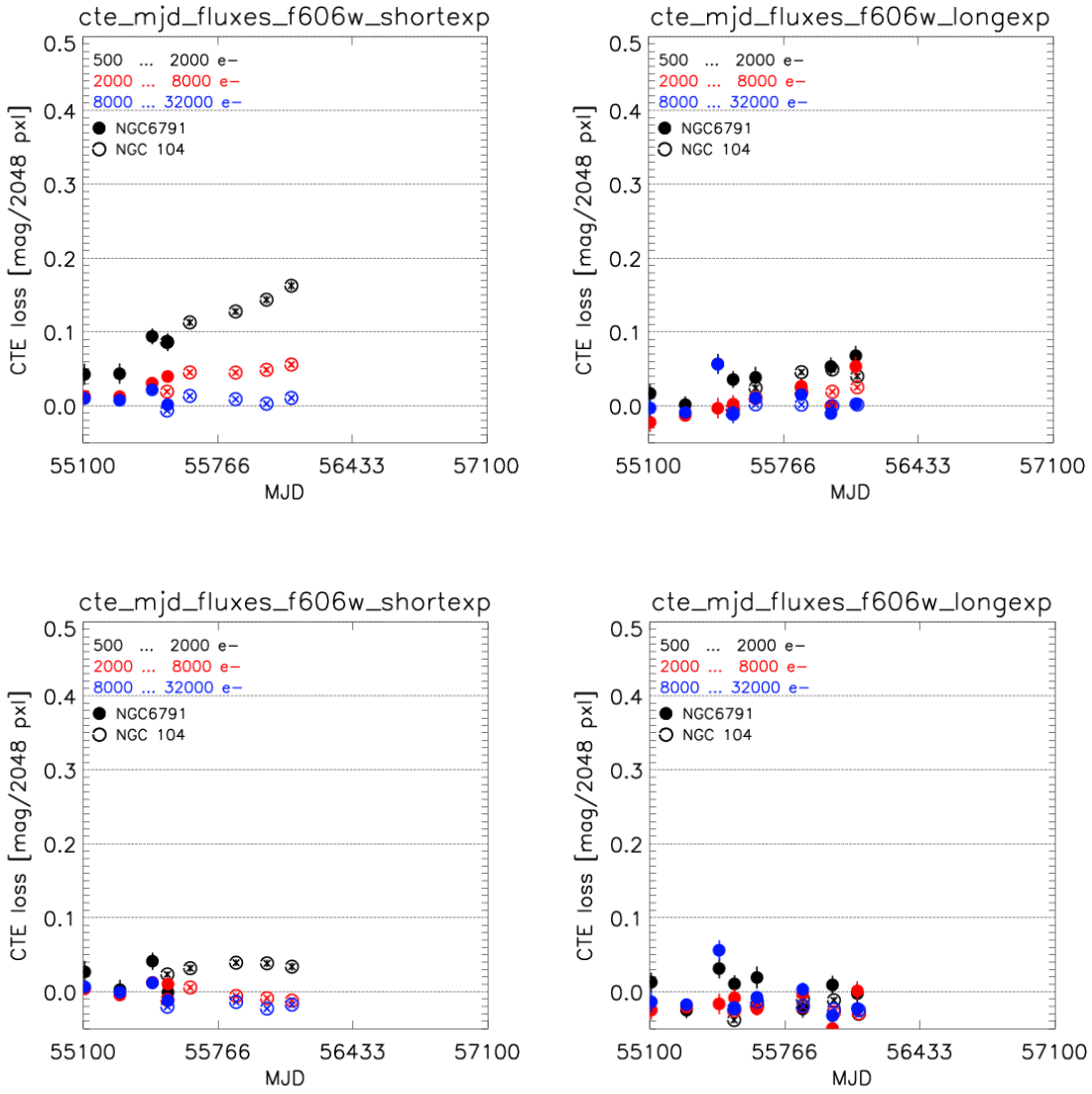

Figure 7. Reduction of CTE losses for broadband F606W images. The top row are the baseline CTE monitor results, i.e. no corrections have been applied, for backgrounds of 2-3 e-/pix and 20-30 e-/pix at left and right, respectively. The bottom row show the data with the pixel-based CTE-correction applied. The F606W observations have been discontinued since Cycle 20, when the post-flash mode became available.

Conclusions

We present the longterm behavior of flux losses due to CTE degradation as a function of the source's distance from the amplifier, source signal level, image background, and epoch of the observations. Worst-case losses occur for faint sources in images with effectively no background, ~50+/-2% as of early 2015; brighter sources show flux losses of 5-15%. Application of a low-level background (with post-flash if necessary) or the pixel-based CTE correction can reduce those losses to 10% for faint sources and 5% or

less for brighter sources. Application of the CTE correction to post-flashed data offers the best CTE moderation especially for fainter and strongly CTE-affected sources, but appears to over-correct the photometry for brighter and less CTE-affected sources by a few percent.

Acknowledgements

We thank Linda Dressel for reviewing and providing helpful comments on this report.

References

Anderson, J., MacKenty, J., Baggett, S., Noeske, K., "The Efficacy of Post-Flashing for Mitigating CTE-Losses in WFC3/UVIS Images," White Paper, Aug 2012, available at http://www.stsci.edu/hst/wfc3/ins_performance/CTE/ANDERSON_UVIS_POSTFLASH_EFFICACY.pdf

Anderson, J., and the WFC3 Team, "Fitting a Pixel-Based CTE Model to the WFC3/UVIS CCD Detector," poster presented at AAS 220th meeting in June 2012. Copy available at http://www.stsci.edu/hst/wfc3/documents/meeting_posters/aas_220/anderson_aas_wfc3cte.pdf

Anderson, J., and Bedin, L., "An Empirical Pixel-Based Correction for HST/ACS," PASP 122, 1035, 2010.

Baggett, S., Bushouse, H., Gilliland, R., Khozurina-Platais, V., Noeske, K., Petro, L., "Charge transfer efficiency (CTE) in the WFC3/UVIS CCDs", Jan 2011, memo available at http://www.stsci.edu/hst/wfc3/ins_performance/CTE/charge_injection/cte.pdf

Baggett, S., and Anderson, J., "WFC3/UVIS Sky Backgrounds", ISR 2012-12, 2012.

Baggett, S., Anderson, J., and Sosey, M., "WFC3/UVIS CTE correction: Requirements for new keywords and reference files", WFC3 Technical Instrument Report 2014-03.

Bushouse, H., Baggett, S., Gilliland, R., Noeske, K., Petro, L., "WFC3/UVIS Charge Injection Behavior: Results of an Initial Test," WFC3 ISR 2011-02, 2011.

Dressel, L., "Wide Field Camera 3 Instrument Handbook, Version 7.0", 2015.

MacKenty, J., and Smith, L., "CTE White Paper", June 2012, available at http://www.stsci.edu/hst/wfc3/ins_performance/CTE/CTE_White_Paper.pdf

Massey, R., et al., "Pixel-based correction for Charge Transfer Inefficiency in HST/ACS", MNRAS 401, 371, 2010.

Noeske, K., Baggett, S., Bushouse, H., Petro, L., Gilliland, R., Khozurina-Platais, V., "WFC3/UVIS Charge Transfer Efficiency October 2009 to October 2011", WFC3 ISR 2012-09, 2012.

Kozhurina-Platais,V., Gilliland, R., and Baggett, S., "WFC3/UVIS Cycle 17: CTE External Monitoring – NGC 6791," WFC3 ISR 2011-06, 2011.

Appendix

As described in Noeske et al. (2012), the functional form of the fit to the CTE slopes is a 2nd order polynomial:

$$S = \sum c_{ij} d^i f^j \qquad (1)$$

where S is the CTE slope, i,j range from 0 to 2, the source flux f is $\log_{10}$flux(e-), and the observation date d is MJD-55400 (July 2010). This expands to

$$S = c_{00} + c_{01}d + c_{02}d^2 + c_{10}f + c_{11}df + c_{12}d^2f + c_{20}f^2 + c_{21}df^2 + c_{22}d^2f^2 \qquad (2)$$

The correction for a given source may be estimated from

$$f_{corr}[mag] = f_{uncorr}[mag] - S * (Y/2048) \qquad (3)$$

where S is computed from equation 2 and Y is the number of rows between the source and the amplifier. The scatter in the data points around the model is generally ~0.01 mag, with a small number of points with scatter ~0.05 mag (Fig 5). Observers may wish to use these coefficients to estimate CTE effects in archival data or to project estimates for future studies. As discussed in the text, flux losses due to CTE effects can be mitigated by ensuring at least 12 e-/pix image background (with post-flash if necessary) and applying the pixel-based CTE correction after the images have been acquired.

Mode Background (e-/pix)	F502N, short ~0	F502N, long ~1-2	F606W, short ~2-3	F606W, long ~20-30
C00	1.73e+00	8.41e-01	8.24e-01	1.15e-01
C01	3.55e-03	2.91e-03	7.91e-04	-5.07e-04
C02	-5.87e-07	-1.17e-06	-6.28e-08	1.18e-06
C10	-8.14e-01	-3.93e-01	-3.83e-01	-5.53e-02
C11	-1.67e-03	-1.40e-03	-3.11e-04	3.41e-04
C12	2.91e-07	6.08e-07	-3.51e-09	-6.37e-07
C20	9.55e-02	4.58e-02	4.48e-02	6.40e-03
C21	1.98e-04	1.68e-04	2.91e-05	-5.09e-05
C22	-3.45e-08	-7.74e-08	4.86e-09	8.37e-08

Table 1. Empirical CTE model coefficients for the monitor data.